CHAPTER 6

FINE-SCALE ULTRA-LOW VELOCITY ZONE LAYERING AT THE CORE-MANTLE BOUNDARY AND SUPERPLUMES

EDWARD J. GARNERO, MICHAEL S. THORNE[1], ALLEN McNAMARA, AND SEBASTIAN ROST[2]

School of Earth and Space Exploration, Arizona State University, Tempe, Arizona 85287-1404, USA; E-mail: garnero@asu.edu

[1]*Now at Arctic Region Supercomputing Center, University of Alaska, Fairbanks, Alaska 99775-6020, USA*

[2]*Now at School of Earth and Environment Earth Sciences, The University of Leeds, Leeds LS6 9JT, UK*

Abstract

Ultra-low velocity layering at the Earth's core-mantle boundary (CMB) has now been detected using a variety of seismic probes. *P*- and *S*-wave velocity reductions of up to 10's of percent have been mapped in a thin (5–50 km) layer, which commonly underlies reduced seismic shear wave speeds in the overlying few 100 km of the mantle. Ultra-low velocity zones (ULVZ) contain properties consistent with partial melt of rock at the very base of the mantle. Strong evidence now exists for a significant density increase in the layer (~5–10% greater than reference models), which must be included in dynamical scenarios relating ULVZ partial melt to deep mantle plume genesis. 3-D geodynamical calculations involving an initially uniform dense layer in the lowermost few 100 km of the mantle result in thermo-chemical piles that are geographically well-correlated with seismic tomography low velocities, when past plate motions are imposed as a surface boundary condition. The hottest lower mantle regions underlay edges of the dense thermo-chemical piles. A scenario is put forth where these piles geographically correlate with ultra-low velocity zones, and subsequent mantle plume genesis.

1 INTRODUCTION

In the past decade increasing evidence has been put forth linking the seismic structure of the deepest mantle to overall mantle dynamics and chemistry on a variety of scale lengths (e.g., 100–3000 km, see Wysession, 1996; van der Hilst and Kárason; 1999; Wysession et al., 1999; Masters et al., 2000; Garnero, 2000; Deschamps and

D. A. Yuen et al. (eds.), Superplumes, 139–158.

Table 1. Seismically observed lower mantle layering features

Deep mantle feature	Thickness at base of mantle (km)	Velocity perturbation (%)		Notes
		δV_S	δV_P	
D″ discontinuity	200–300	2 to 3	$\sim< 1$	δV_P discontinuity difficult to detect
D″ anisotropy	200–300	1 to 2	Unconstrained	Mechanism still poorly resolved
ULVZ	5–30	−10 to −30	−5 to −10	ULVZ density an important parameter
Large low velocity provinces	500–1500	−3 to −12	−1 to −3	Sharp sides, likely chemically distinct

Trampert, 2003; Lay et al., 2004; Lay and Garnero, 2004). It has been known for over 50 years that the structure of the lowermost few hundred km of the mantle, the D″ region (Bullen, 1949) differs from overlying mantle structure. Recent studies using regional forward modeling of seismic waveforms and travel times reveal complex structure on a variety of both radial and lateral scale lengths, in contrast to the bulk of the lower mantle. Features detected in D″ include evidence for a seismic velocity discontinuity (the D″ discontinuity) some 200–300 km above the CMB (e.g., see Wysession et al., 1998), anisotropy in the lowermost few 100 km of the mantle (e.g., Kendall and Silver, 1998; Lay et al., 1998; Kendall, 2000), as well as thin ultra-low velocity layering in the deepest 5–50 km of the mantle (e.g., see Thorne and Garnero, 2004). The seismic characteristics of these features are summarized in the Table 1. A principal challenge is to constrain the origin of these features, as well as their possible connection to the evolution and dynamic behavior of the lower mantle. In this regard, incorporating information from other geophysical disciplines will be crucial.

For decades, the general presence of two long wavelength low velocity regions at the base of the mantle has been noted (e.g., Dziewonski, 1984; Romanowicz, 1991). This degree-two pattern of velocity reductions is particularly evident for shear velocities (V_S). These low velocity regions generally underlie the locations of surface hot spot volcanism, and do not underlie regions of past or present subduction (e.g., Morgan, 1971, 1972; Hager et al., 1985; Duncan and Richards, 1991), suggesting an interaction between the shallowest and deepest mantle. The large-scale low velocities detected through seismic tomography have been dubbed "super" or "mega" plumes (e.g., Tackley, 2000). However, it has not been demonstrated that these low-velocity regions actually constitute a plume (as in upwelling) as opposed to a pile (as in some form of dense and possibly stable dreg).

One challenge in distinguishing between a plume upwelling and stable dense pile lies in the difficulties of seismically resolving the detailed nature of high- or low-velocities in the mid-mantle. Tomographic imaging typically resolves structure on the order of 1000+ km laterally (see Fig. 1), while plumes may be an order of magnitude smaller. For example, a plume conduit in the mid mantle could have a diameter of roughly 100–400 km (e.g., Ji and Nataf, 1998). Although tomographic imaging

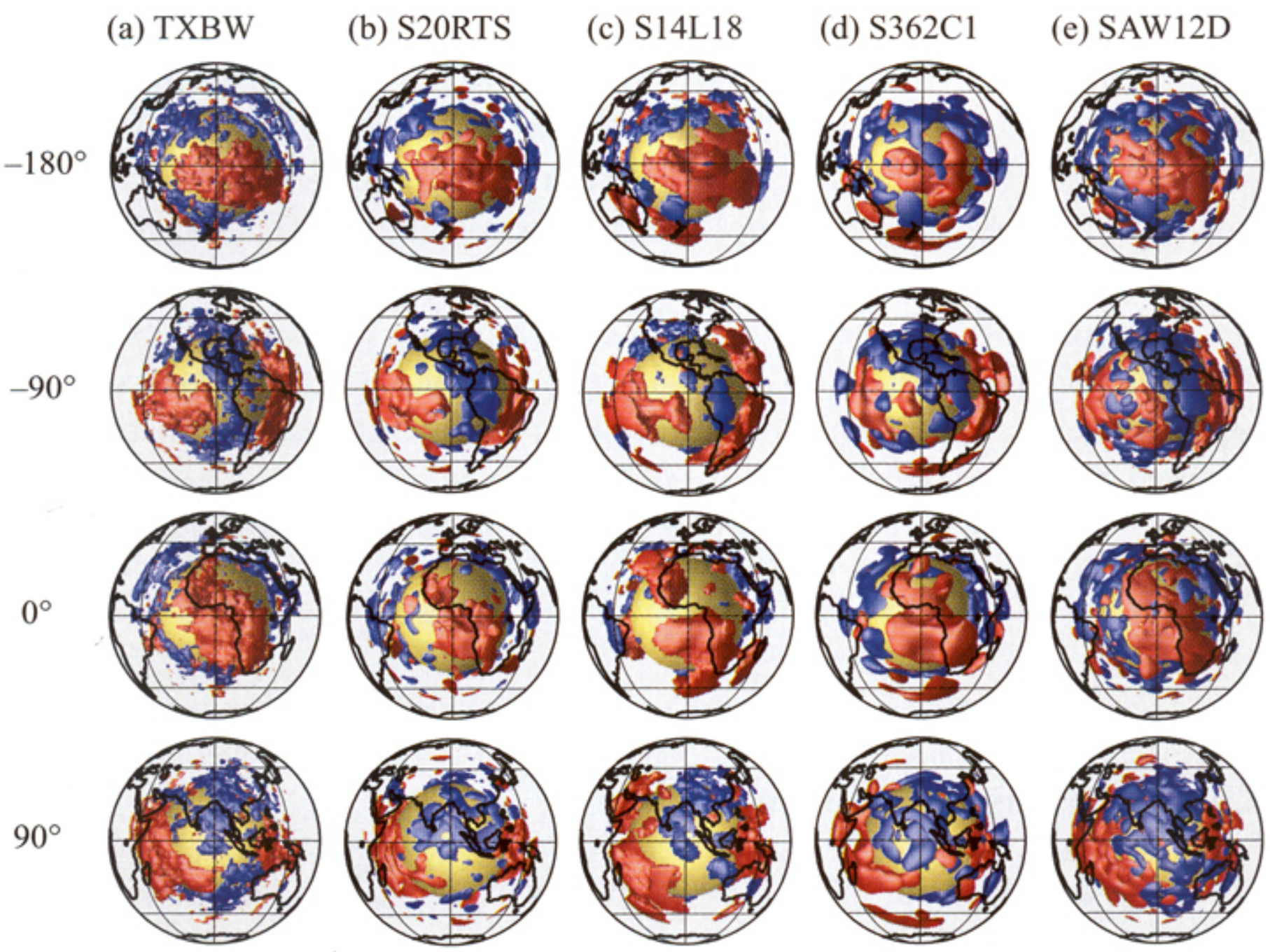

Figure 1. Iso-contoured shear velocity heterogeneity in the lower mantle from five different tomographically derived models: (a) TWBX (Grand, 2002), (b) S20RTS (Ritsema and van Heijst, 2000), (c) S14L18 (Masters et al., 2000), S362C1 (Gu et al., 2001), and SAW (Mégnin and Romanowicz, 2000). Iso-velocity surfaces are shown, where the low velocity (red) and high velocity (blue) surfaces represent at −0.8 and +0.8%, respectively, relative to global 1-D reference velocity structures. Longitude of the viewing perspective is shown to the left of each row. The −180° and 0° views display the degree 2 low shear velocity anomalies beneath the Pacific Ocean and southern Atlantic Ocean/Africa, respectively. Iso-velocity contours are shown for the bottom 1800 km of the mantle. The core-mantle boundary is shown in yellow.

has typically been unable to resolve structures with length scales as small as plume conduits, recent finite frequency based tomographic imaging of Montelli et al. (2004) reports mapping of low compressional velocities (V_P) from the Earth's surface to large mantle depths beneath several hot spots. At the time of this writing, tomographic imaging of V_S structure has not yet corroborated this result.

Body wave studies are able to provide a greater level of detail in seismic imaging than tomography, especially near the core-mantle boundary (CMB) where various reflections, refractions, and diffractions of seismic energy occur. However, a main restriction in high-resolution body wave studies is the geographic coverage limitations imposed by earthquake-to-seismic recording network configurations. It is particularly challenging if high numbers of seismometers (e.g., >20) are desired over small surface spatial scales (e.g., <100–300 km). Nonetheless, recent body wave analyses have complemented the earlier findings from tomographic inversions of global travel time data sets, adding detail to some of the long wavelength features observed in tomographic models (see recent discussions by Lay et al., 2004; Lay and Garnero,

2004; Garnero, 2004). One notable example is the evidence for multi-pathing (i.e., the presence of two distinct seismic arrivals) in broadband data that sample near the edge of the African low-Velocity anomaly (e.g., Helmberger and Ni, 2005). Multi-pathing is consistent with a sharp (i.e., 10's of km) transition from ambient mantle into the low velocity region. Similar evidence now exists for the Pacific Ocean low velocity anomaly (Ford et al., 2006; To et al., 2005).

In the remainder of this chapter, we discuss scenarios that relate these large-scale low velocity provinces to ultra-low velocity zone (ULVZ) structure and whole mantle plumes. At present, considerable uncertainty exists in precisely constraining elastic properties through seismic imaging, and hence propagations uncertainties to the geodynamic modeling. However, several possibilities can be discussed that form a self-consistent dynamical and chemical system.

2 DEEP MANTLE SEISMIC AND GEODYNAMIC STRUCTURES

2.1 Long wavelength deep mantle patterns

As displayed in Figure 1, large-scale features dominate tomographically derived S-wave velocity perturbations in the lower mantle. Many regional seismic studies have documented structure at scales much smaller than those seen in Figure 1 (see review by Garnero, 2000). It is still unresolved whether tomography accurately depicts the general shape of deep mantle heterogeneity or a smoothed version of much smaller scale, higher amplitude heterogeneity. Nonetheless, several higher resolution studies using waveform and travel time information have recently documented sharp edges to the low velocity patterns seen in tomography (Wen, 2001; Ni et al., 2002; Ni and Helmberger, 2003a,b; Helmberger and Ni, 2005; Ford et al., 2006; To et al., 2005). Thus, the general shapes of the degree-two lows seen in tomography may in fact approximate a smoothed version of Earth's large-scale velocity reductions in the deepest mantle. Though it is important to emphasize that regional studies do not mandate this possibility.

It is instructive to compare various available deep mantle seismic and geodynamic findings, in order to better understand possible dynamical implications of the detected seismic structures, particularly as they relate to ULVZ's. Figure 2a shows D″ shear velocity perturbations (δV_S) for the TXBW model (as in Fig. 1a). Only heterogeneities with amplitudes stronger than $\pm 0.5\%$ are shown. The edges of the degree two low velocity anomalies in this tomographic study contains the strongest lateral gradients in shear wave speeds (as shown in Fig. 2b); these regions of strongest S-wave velocity lateral gradients show a strong correlation to surface hot spot volcanism locations (Thorne et al., 2004), and are detected far from predicted deep mantle locations of subducted material (Fig. 2c). This suggests a connection between subduction and lower mantle structure, that is, whole mantle convection. Furthermore, the strong lateral velocity gradients at the edges of the lowest-velocity regions of the lower mantle point towards the existence of thermo-chemical heterogeneity as source for the detected low velocities.

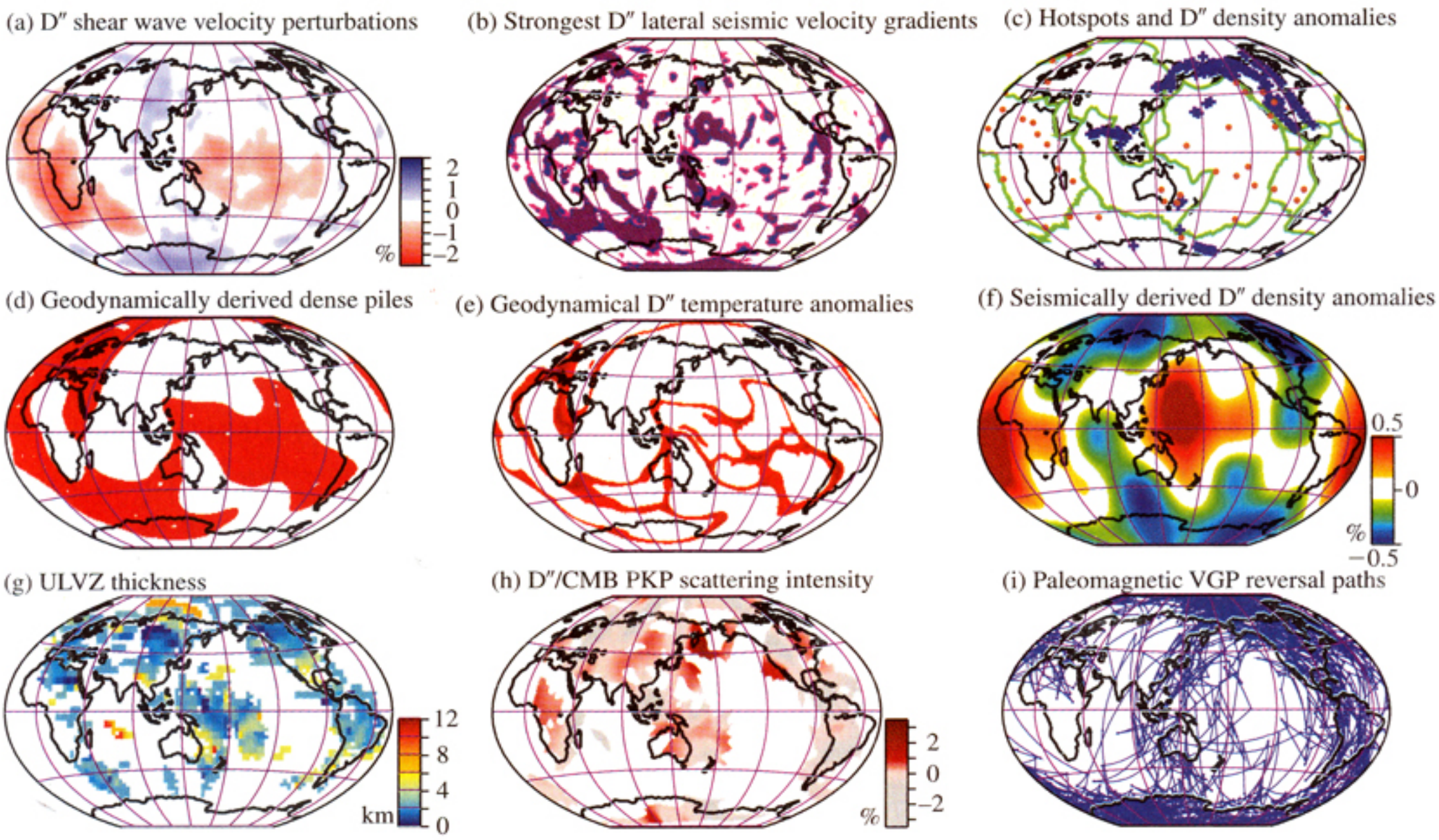

Figure 2. Comparison of several deep mantle data sets and models: (a) D″ shear velocity perturbations according to the TWBX model (Grand, 2002). The values between −0.5 and +0.5% have been omitted to emphasize the stronger heterogeneity signals. (b) The lateral gradients in δV_S of panel (a), as measured in Thorne et al. (2004). The colors correspond to the 30% of the CMB's surface area occupied by the strongest lateral gradients. These patterns, when compared with panel (a), indicate the strongest gradients in D″ surround the low shear velocities, i.e., the edges of low velocities. (c) Hotspots (red), plate boundaries (green), and predicted deep mantle locations of subducted dense material (from Lithgow-Bertelloni and Richards, 1998). (d) Dense thermo-chemical piles from the numerical geodynamics calculations of McNamara and Zhong (2005). The highest temperatures in these simulations are shown in (e), which dominate the edges of the dense piles in (d), along with some lineations within piles that demark internal convection cells. (f) Predicted lower mantle density anomalies of Trampert et al. (2004). (g) ULVZ thickness, assuming $(\delta V_P, \delta V_S, \delta\rho) = (-10\%, -30\%, 0\%)$, adapted from the modeling of Thorne and Garnero (2004). The thickest ULVZ regions are red. (h) PKP scattering strength from Hedlin and Shearer (2000). The strongest scattering occurs for the red colors.

Thermochemical mantle models are geodynamically attractive to explain the large degree two negative seismic anomalies in the lower mantle because geodynamical modeling of isochemical systems has revealed that hot upwellings tend to form more-globally ubiquitous small scale structures (e.g., Bunge et al., 1998, 2002). In other words, past studies have demonstrated the difficultly in generating two large thermal anomalies by thermal convection alone. Several geodynamical studies have been performed that investigate the 3-D morphology and size of possible thermochemical structures in the deep mantle (Olson and Kincaid, 1991; Tackley 1998, 2002; Davaille 1999; Davaille et al., 2002, Jellinek and Manga, 2002, 2004; McNamara and Zhong, 2004a,b, 2005). Depending on the thermochemical parameters used, a dense mantle component will take the form of either rounded, rising, unstable superplumes or linear, stable piles. Under the assumption that stable, dense piles

exist in the lower mantle, McNamara and Zhong (2005) have performed fully 3-D spherical numerical thermochemical convection calculations which incorporate the Earth's 120 My tectonic plate history (from Lithgow-Bertelloni and Richards, 1998) as surface boundary conditions. Starting with initially uniform dense layers of various thicknesses and density contrasts (~2–5%), the final shape and distribution (representing the present day) of thermochemical piles as a function of this plate history forms tends to resemble to first order the large, negative seismic anomalies observed in tomography. It is found that resultant thermochemical piles form a NW-SE trending linear African pile. In contrast, dense material forms a superposition of linear piles in the Pacific resulting in a more-rounded structure there. Also, thermochemical piles tend to have a low cooling efficiency and are therefore large thermal anomalies in addition to being compositional anomalies.

In addition, the geodynamical models predict internal convection within the Pacific anomaly in which upwellings form inside the pile along the edges, likely guided by viscous coupling with the less-dense mantle component. As a result, the internal edges of thermochemical piles are expected to be the hottest regions in the mantle, and if there is any partial melting in the lower mantle, it would certainly be expected to occur inside thermochemical piles at their edges. It is interesting to note the conceptual agreement between the spatial correlation of the strongest lateral velocity gradients in δV_S (Fig. 2b) occurring near the edges of the low δV_S piles (Fig. 2a), and the highest deep mantle temperatures (Fig. 2e) occurring near the edges of the high density thermo-chemical piles (Fig. 2d).

As observed in the previous geodynamical modeling studies, upwellings are produced at the highest peaks of thermochemical piles or superplumes. The modeling of McNamara and Zhong (2005) predicts a Pacific anomaly which is actually a superposition of linear ridges. The ridges form the external edges of the complete anomaly, and as a result, the modeling predicts mantle plumes to form along the tops of these ridges. Therefore, the highest number of mantle plumes in the Pacific is expected to form near the edges of the large Pacific anomaly.

Several further lines of evidence exist for the large scale δV_S depressions shown in Figure 1 and Figure 2a having a chemical origin that is distinct from the surrounding lower mantle material (e.g., see arguments by Samuel et al., 2005). The V_P and V_S velocity perturbation maps appear to be decoupled; including portions of the degree 2 low δV_S having anomalously high P wave speeds (Masters et al., 2000; Deschamps and Trampert, 2003; Ishii and Tromp, 2004; Trampert et al., 2004). It seems unlikely that the decoupling of P and S-wave velocities could solely be the result of thermal perturbation in an isochemical lower mantle. Furthermore, it seems unlikely that sharp lateral transitions (e.g., probably near or less than 100 km) in the low δV_S anomalies can be maintained over extended periods of time by thermal effects. On the other hand chemical variations can easily explain the observed structure as some form of iron enrichment may relate to the lowered shear wave speeds, increased density, and hotter temperatures in this region. We note though that at present no consensus on the origin and constitution of the potentially dense, low-velocity piles has been reached.

Several groups have put forth evidence for density perturbations in the deep mantle (e.g., Masters et al., 2000; Ishii and Tromp, 1999, 2004, Trampert et al., 2004), though some controversy exists regarding the details (Kuo and Romanowicz, 2002; Masters and Gubbins, 2003). Figure 2f shows a density perturbation model of Trampert et al. (2004), which is appropriate for the lowest 1000 km of the lower mantle. The pattern seen in this particular density map roughly correlates well with the geographical locations of the δV_S reductions, though trade-offs in density modeling have been highlighted in previous modeling (e.g., Deschamps and Trampert, 2003; Trampert et al., 2004). Better constraint on the density structure of the degree 2 low velocity anomalies is important, as it relates to a fundamental question regarding the nature of these structures. They have been characterized as "superplumes" for over a decade now (e.g., Su and Dziewonski, 1997), but if they are dense and stable at the base of the mantle and not actively upwelling (as buoyant plumes would do), they may be more appropriately characterized as "piles", or "megapiles" (e.g., Tackley, 1998, 2002; McNamara and Zhong, 2004a). In this chapter, we further explore the megapile possibility, since dynamical calculations have shown the necessity of high densities (along with elevated viscosity) in order to reproduce the long wavelength shape of the degree 2 δV_S reductions (e.g., Tackley, 1998, 2000; McNamara and Zhong, 2004a). We are nonetheless aware that the existing seismological data are presently not sufficient to constrain the detailed internal structure of the low-velocity features. We note an additional inherent shortcoming in seismic imaging of Earth's interior that restricts its application to geodynamical problems: at best, a present day snapshot in time is all that is available. Thus, unfortunately, we are not able to constrain the temporal evolution or specific time signatures of the different seismic features.

2.2 Short wavelength deep mantle patterns

A variety of phenomena have been seismically mapped in the deep mantle at scale lengths much shorter than tomographically derived heterogeneity. These include strong variability in horizontal layering and anisotropy (e.g., see Wen, 2001; Rokosky et al., 2004; Thomas et al., 2004; Garnero et al., 2004), and highly variable ULVZ and CMB properties (e.g., Shearer et al., 1998; Rost and Revenaugh, 2001, 2003; Niu and Wen, 2001; Koper and Pyle, 2004; Rondenay and Fischer, 2003; Thorne and Garnero, 2004; Wang and Wen, 2004; Rost et al., 2005). The lateral gradient map in Figure 2b shows small-scale features that cannot be observed in the δV_S maps. Nonetheless, this is expected for a derivative of the data, rather than actual detected small-scale structure. Figure 2g displays ULVZ thickness, from the modeling experiments in Thorne and Garnero (2004) using diffracted phases as probes to ULVZ structure. Roughly one-third of the CMB is sampled, and these results argue that the ULVZ is not globally contiguous as a relatively thick layer (e.g., >5 km). In fact, it appears that the ULVZ structure is most anomalous in relatively localized regions. For example, very localized, anomalous (i.e., thick ULVZ) regions exist in the Indian Ocean and between New Zealand and Australia with lateral dimensions

of 100–200 km. The Australian location was imaged as having a ~50 km lateral dimension ULVZ in a recent study by Rost et al. (2005) using short period seismic array recordings of hundreds of Fiji-Tonga earthquakes. It is obvious that significant heterogeneities exist at scales more than an order of magnitude less than presently resolvable by tomography, which nonetheless can be resolved by high resolution, regional studies.

Another expression of small-scale heterogeneity found in the seismic wavefield is scattering of seismic energy. It has been appreciated for some time that the D″ region has an exceptionally strong scattering potential for short period seismic energy (e.g., Bataille et al., 1990; Bataille and Lund, 1996; Flatté and Wu, 1988; Vidale and Hedlin, 1998; Hedlin and Shearer, 2000; Cormier, 1999, 2000). Figure 2h displays the results of a study imaging D″ (or CMB) scattering strength, using PKP precursors (Hedlin and Shearer, 2000). An important point is that the variations are much smaller (~500 km) than in global tomography (~1000–3000 km), although the exact magnitudes of scattering strength depend on several factors in the inversion. Strong scattering regions (red colors) are difficult to correlate to specific features in the other maps. A comparison with global features found in the other geophysical studies shown in this figure is not possible since the scatterer map is not globally continuous Nonetheless, comparison with ULVZ thickness (Fig. 2g) suggests the thickest ULVZ zones are closer to high scattering zones than not. This suggests that the possibly partially molten ULVZ may be related to small scale stirring, that give rise to effective scattering at short seismic wavelengths (~1 Hz).

It is instructive to view ULVZ structure in a well-sampled region in the southwest Pacific. Figure 3 shows the combined findings of different ULVZ studies. Figure 3a displays the δV_S tomography map of Grand (2002), along with CMB sampling of ScP data with or without precursors, which have been used to map a very localized ULVZ (~50 km in lateral dimension, 8.5 km thick, and V_P and V_S drops of 8 and 25%, respectively, and density increase of 10%) (Rost et al., 2005). This ULVZ is located close to the edge of the low shear velocities mapped by tomography (Figs. 3a, and 2a). This ULVZ location is also in a region of strong lateral δV_S gradients (Fig. 2b), and where the temperatures in the geodynamical calculation (Fig. 2e) are predicted to be the highest (beneath the edge of the thermochemical dense pile, Fig. 2d). This isolated ULVZ location is corroborated by the anomalous waveform behavior of SPdKS data (Fig. 3b) (from Thorne and Garnero, 2004). These data commonly vary on the lateral scales of 10's of km at the CMB. At a scale intermediate to this fine scale variability and that seen in tomography, Fresnel zones of SPdKS can be used to represent ULVZ likelihood, a simple measure of records requiring a ULVZ structure versus records best explained in the absence of a ULVZ (Fig. 3c); this general region displays high variability in ULVZ likelihood. Thus, if ULVZ are indeed related to very local thermal and chemical anomalies in the dense thermo-chemical piles, it is natural to expect high variability at the shortest scales in the ULVZ structure. It is noteworthy that even finer scale CMB structure may exist. For example, a region a few 100 km to the north has been mapped with a core-side localized anomaly (Rost and Revenaugh, 2001). Thus we further allow for the possibility that the core-mantle

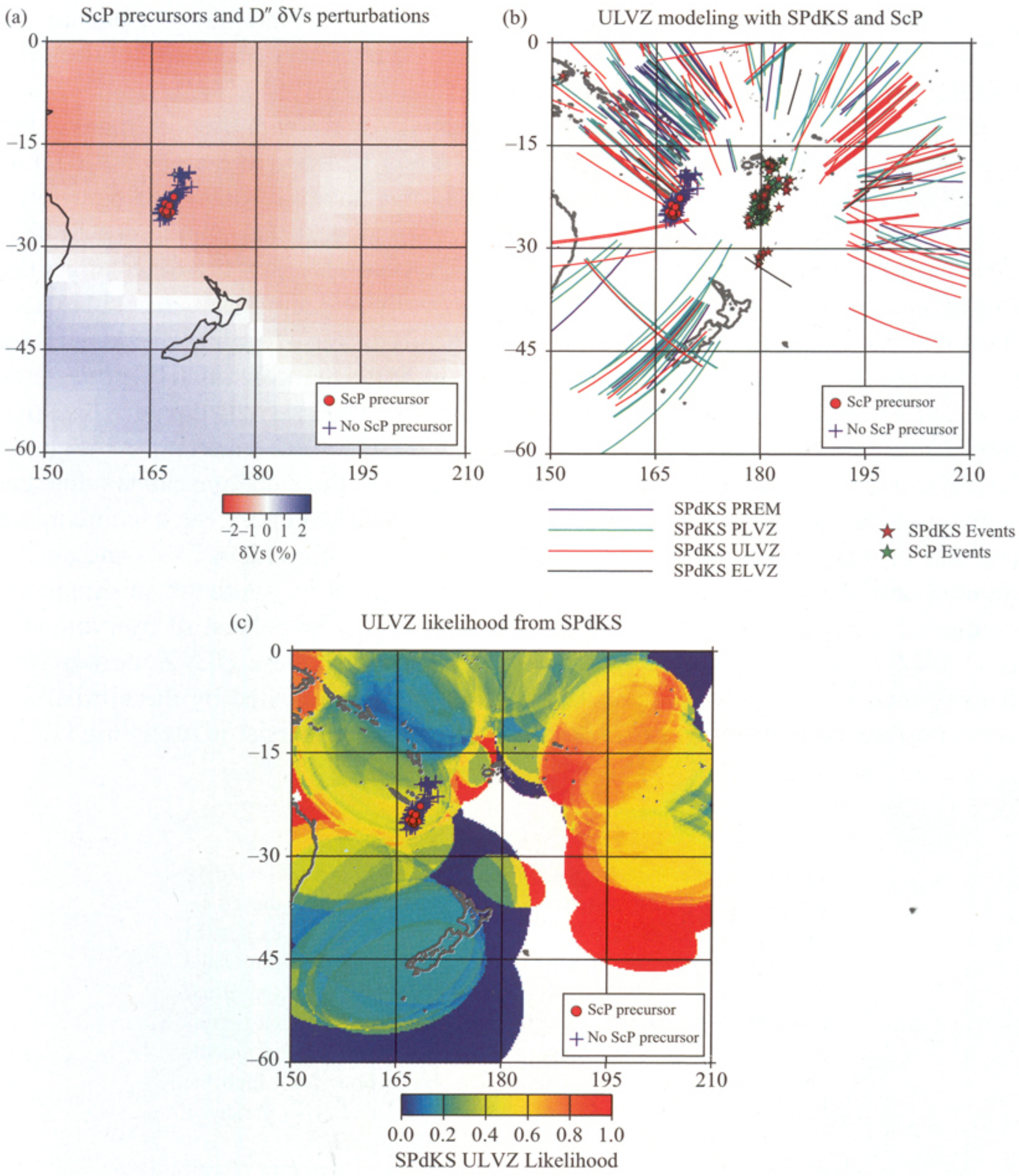

Figure 3. ULVZ behavior in the southwest Pacific (the region shown includes New Zealand and eastern-most Australia). (a) δV_S of Grand (2002) with ScP sampling of Rost et al. (2005) also shown, indicating a CMB zone possessing a very localized ULVZ (red circles). (b) The same ScP data, displayed with SPdKS data of Thorne and Garnero (2004), which also show strongly anomalous behavior in this general region. Line segments correspond to the P_{diff} arcs in SPdKS. Paths are color-coded for: PREM (fpr the Preliminary Reference Earth Model, Dziewonski and Anderson, 1981, shown as blue lines, indicating no ULVZ), PLVZ (Probable Low Velocity Zone, based on a statistical measure of the improvement of fit to the data from ULVZ predictions compared to PREM, light green), ULVZ (red), and ELVZ (Extreme Low Velocity Zone, where records were more anomalous than any of our tested ULVZ structures, colored black). (c) ScP data as in (a), superimposed on top of Fresnel zone estimations of the P_{diff} arcs in SPdKS, color-coded for ULVZ likelihood, as measured by a simple ratio of the number of records requiring ULVZ models to match the data divided by the total number of records, in every $5° \times 5°$ region.

transition (and not just fine layering above it) is extremely anomalous, especially in regions as depicted in Figure 3, which may include chemical reactions between the mantle and core material (e.g., Knittle and Jeanloz, 1989, 1991).

Synthetic seismograms computed for the ScP waveform data used in imaging the SW Pacific ULVZ by Rost et al. (2005) required an increase in density (+10%) of the ULVZ in order to fit the waveforms. Further evaluation of data used by Thorne and Garnero (2004), summarized in Table 2, also suggest that anomalous SPdKS data are best fit by models containing density increases. Density increases affect the impedance contrast between the ULVZ and the overlying mantle, which (a) increases the relative amplitude ratio between the reflection off the top of the ULVZ and ScP, and (b) increases the amplitude of an internal ULVZ multiple that constructively interferes with SPdKS relative to SKS. The Thorne and Garnero (2004) study did an exhaustive model space search to characterize constraints, trade-offs, and uncertainties in global ULVZ modeling. To assess general ULVZ model fits to the data, one can tabulate the number of data that are well fit by any particular model category, such as including (or not) an elevated density in the ULVZ, mantle or core-side ULVZ, and so on. Table 2 shows that 154 individual records were best fit by synthetic seismograms computed for ULVZ models. Of these 154 records, 106 were best fit by synthetics for ULVZ models with a density increase. Furthermore, these ULVZ models with density increases display the best data-to-model fit as indicated by the normalized cross-correlation coefficient in Table 2. Although tradeoffs exist in modeling ULVZ

Table 2. ULVZ modeling misfit statistics. Misfit is represented by the average (for all observations) difference between the cross-correlation coefficient (CCC) of each observation and its best fit (bf) synthetic seismogram (CCC^{bf}) and the CCC of the same observation and models of the model class categories (m) listed below (CCC^{m}). Thus larger misfit numbers indicate poorer performance of this model or class of models in comparison to models best fitting the whole data set. Only observations for which the best-fit model had a $CCC > 0.85$ were included. This yielded a total number of records (NR) of 273

Model type	Misfit ($< \overline{CCC} >$[a])	NR_{bf}[b]
PREM	4.85	47
ULVZ ($\delta\rho = 0$)	0.72	48
ULVZ ($\delta\rho > 0$)	0.30	106
ULVZ ($\delta V_S = \delta V_P$)	0.52	119
ULVZ ($\delta V_S = 3\delta V_P$)	1.16	35
CRZ	0.59	57
CMTZ	1.47	15

[a] $<\overline{CCC}> = \dfrac{\sum_{i=1}^{n}\left(CCC_i^{bf} - CCC_i^{m}/CCC_i^{bf}\right)*100\%}{n}$.

[b] NR_{bf} – Number of records best fit by this model space.

properties such as density (e.g., Garnero and Helmberger, 1998), these ScP and SPdKS data sets both indicate that to adequately model ULVZ structure elevated densities are typically necessary.

3 THERMO-CHEMICAL AND GEODYNAMICAL POSSIBILITIES

A connection between dense thermo-chemical piles in the deep mantle and depressed seismic shear wave speeds has been suggested (McNamara and Zhong, 2005). Here, we have raised the possibility that ULVZ may be more likely to occur near the edges of such lower mantle features, as the highest deep mantle temperatures may be located there (Fig. 2). In this section, we further explore the possible origins of generating a ULVZ, and how this might relate to other important mantle processes.

For nearly a decade, it has been argued that the 3 to 1 reduction of δV_S to δV_P in the ULVZ indicates a partial melt origin, based on mineral physics grounds (e.g., Williams and Garnero, 1996; Berryman, 2000; Akins et al., 2004), and that this relates to plume genesis from the ULVZ layer, which is manifest in the high correlation of surface hotspots and ULVZ structure (Williams et al., 1998). A recent revisiting of this topic has revealed that hotspots are in fact more likely to overlie the strongest lateral gradients in δV_S (Thorne et al., 2004). Thus, ULVZ structure can indeed be related to plume initiation at or near the CMB. Though it is important to acknowledge that plumes are likely be perturbed from vertical conduits due to mantle convection (e.g., Steinberger, 2000); exactly to what extent is unresolved at present.

Several possible relationships between ULVZ and lower mantle structures are explored in Figure 4. Important considerations are: (i) is the ULVZ partial melt of some principle D″ component, such as post-perovskite structure silicate (Murakami et al., 2004; Tsuchiya et al., 2004; Oganov and Ono, 2004; Shim et al., 2004), or dense thermo-chemical piles (Tackley, 1998; 2000; McNamara and Zhong, 2004a) or layering (Lay et al., 2004; Lay and Garnero, 2004); (ii) is the ULVZ some distinct material, such as chemical reaction products between the mantle and core (e.g., Poirier, 1993; Song and Ahrens, 1994; Manga and Jeanloz, 1996); or (iii), is the ULVZ regionally localized, or global, being imperceptibly thin in regions. The scenarios in Figure 4 are meant to be provocative, illustrating some of the end-member possibilities, though certainly not exhaustive, mainly owing to the lack of solid constraints on elastic structure that would help to distinguish between scenarios. Though it is important to note that present methods would not be able to detect a ULVZ layer less than a few km thick, unless its properties were exceedingly anomalous (e.g., see Garnero and Helmberger, 1998; Thorne and Garnero, 2004; Rost and Revenaugh, 2003; Rost et al., 2005).

While there has been a suggestion that partially molten ULVZ material may relate to plume genesis, it is perhaps premature to seismically constrain the connectivity of whole mantle (or nearly whole mantle) plumes to deep mantle superplumes. The work of Montelli et al. (2004) has mapped low velocity conduits throughout the mantle in key locations, but do not show evidence for large scale deep mantle superplumes (or megapiles) underlying the conduits. Shear velocity tomography models (e.g., Fig. 1)

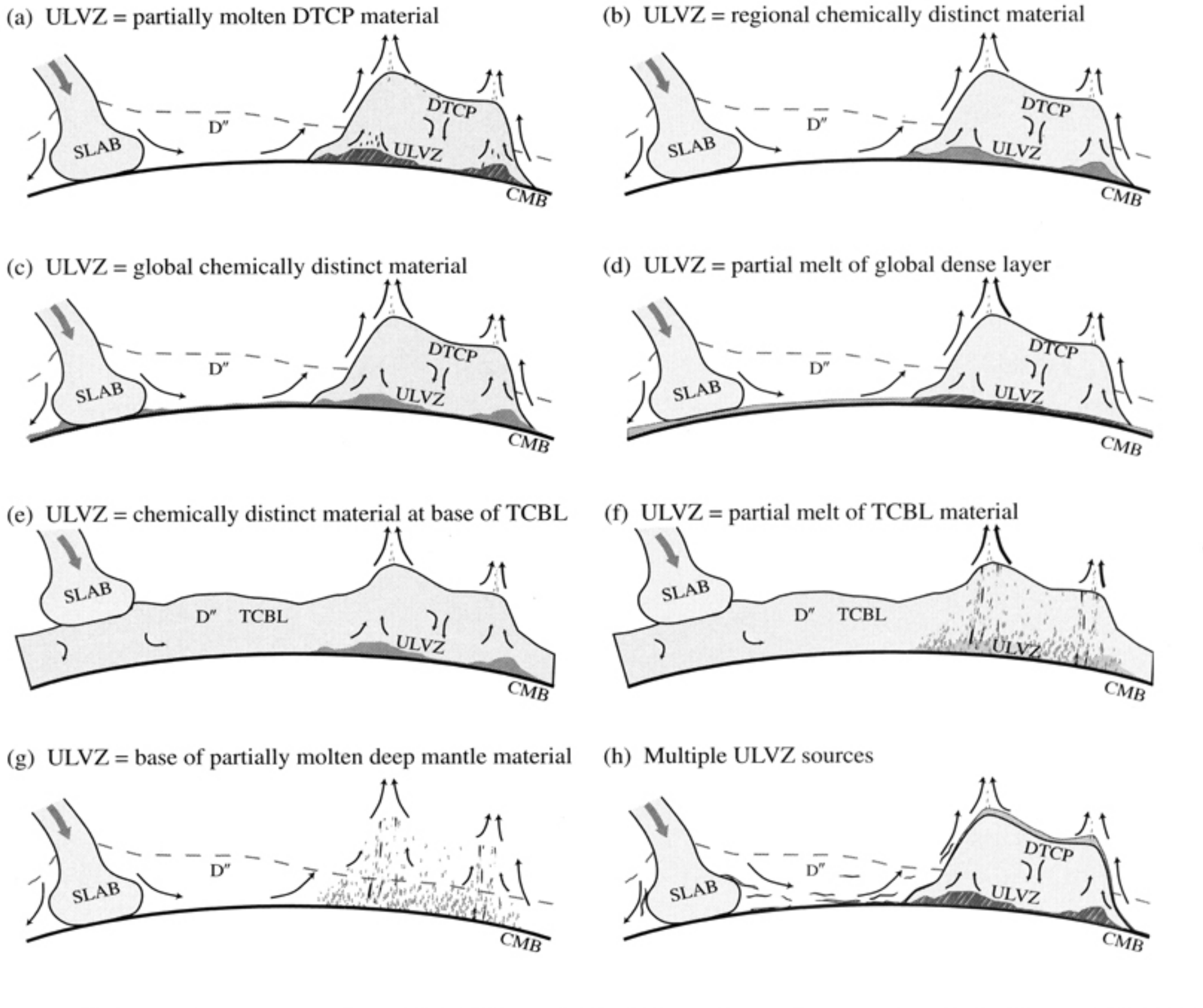

Figure 4. Schematic representation of ULVZ in relationship to dense thermo-chemical piles, or "DTCP", global thermo-chemical layering, and a purely thermal possibility. The different panels are intended to highlight the various possibilities of ULVZ as either chemically similar or distinct from its surrounding rock. (a) ULVZ is partially molten DTCP material, and thus is geographically restricted to DTCP regions. (b) As in (a), but the ULVZ material is distinct from DTCP. (c) ULVZ is a global chemically distinct (and dense) layer, it is thickest (and detectable) in the hottest deep mantle regions. (d) As in (c), except the ULVZ is detectable owing to partial melt of the dense layer. (e) ULVZ is chemically distinct, and ponds beneath the hottest regions in a global thermo-chemical deep mantle layer. (f) The ULVZ is partial melt of a global thermo-chemical lower mantle layer. In this panel the partial melt is portrayed as mixing throughout the layer. (g) ULVZ is partial melt of the post-perovskite material. (h) The possibility of multiple ULVZ sources is portrayed, combining (a) with dense melt from former harzburgitic oceanic crust delaminating from descending slabs.

show evidence for the degree 2 anomalies, but resolution is not quite high enough to track smaller scale plumes from these features up through the mantle. We anticipate important advances in this area over the next several years as data coverage increases in important areas, such as the central Pacific.

Nonetheless, insight from geodynamical numerical calculations and laboratory experiments provide important starting points for synthesizing the seemingly diverse results from seismic studies. Plumes appear to most easily generate from topographical ridges or points (e.g., Jellinek and Manga, 2002, 2004; McNamara and Zhong,

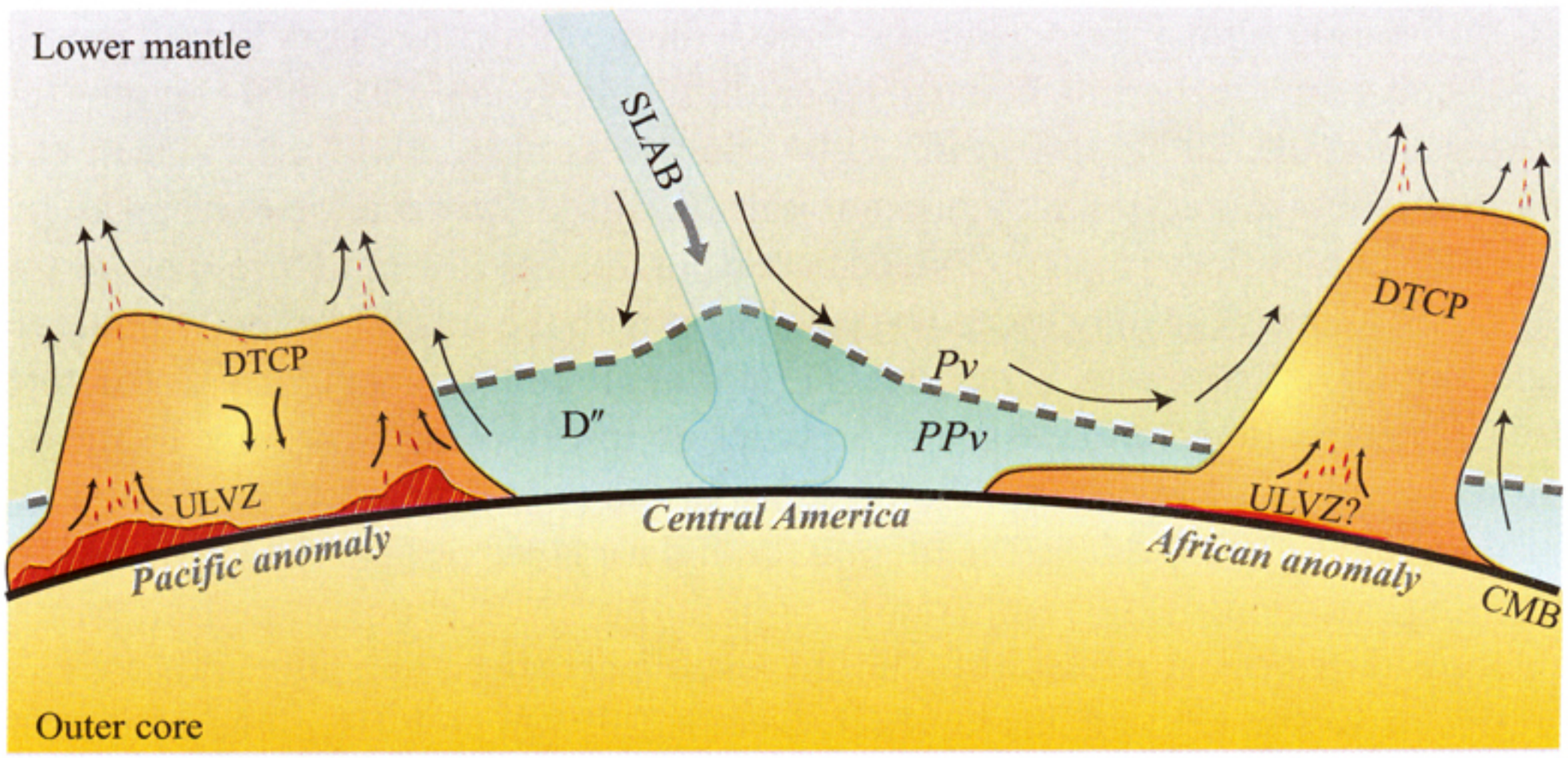

Figure 5. Hypothetical west-to-east cross-section (viewing to the north, approximately equatorial) of the lower mantle that incorporates dense thermo-chemical piles (DTCP), ultra-low velocity zones (ULVZ), and the perovskite (*Pv*) to the post-perovskite (*PPv*) structure solid-solid phase change (dashed line is the implied phase boundary). ULVZ are within the DTCP, which contain the hottest lower mantle temperatures; overlying ridge like topography atop the DTCP is the most likely location for mantle plume initiation.

2004a; 2005). Thus, ridges near the edges of dense thermo-chemical piles that overly the hottest deep mantle areas and possibly ULVZs (see Fig. 2), may be the most likely zones for mantle plume initiation. Figure 5 reiterates this possibility for a hypothetical cross-section across the equator from the Pacific through Central America and through to Africa. Extensive evidence exists for ULVZ beneath portions of the Pacific low-velocity anomaly, but ULVZ underplating of the African anomaly is less clear. The work of Ni and Helmberger (2003a, b) and Helmberger and Ni (2005) argue for the absence of any ULVZ layering, while Wen (2001) and Wang and Wen (2004) (for example) argue that the base of the large African anomaly has shear velocity reductions up to −12%, which is essentially a mild ULVZ structure. Thus, Figure 5 leaves open the possibility that the African anomaly may be distinctly different from the Pacific anomaly.

4 DISCUSSION

Other important possibilities exist for the nature of large scale upwellings in the mantle, i.e., superplumes, which potentially have far reaching consequences (Maruyama, 1994; Maruyama et al., 1994). Several shapes to upwellings are possible, and include the possibility of only a weak seismic signature of the excess plume temperature (e.g., Farnetani and Samuel, 2005). The recent important discovery of the post-perovskite phase (see summary by Lay et al., 2005) must also be considered in relationship to ULVZ, as this is potentially the dominant lower mantle mineral on the mantle side of

the CMB. While significant seismic and geodynamic evidence exists for the presence of lowermost mantle thermochemical anomalies, at large and short scale lengths (e.g., see Masters et al., 2000; Lay et al., 2004; Saltzer et al., 2004; Van Thienen et al., 2005; Samuel et al., 2005), a significant portion of the deep mantle (i.e., away from the degree 2 low velocities) may indeed be the post-perovskite structure. The partially molten post-perovskite may indeed be consistent with the seismic velocity reductions imaged for ULVZ structure. Though it is important to reiterate that ULVZ structure is more commonly detected in association with the lower velocity regions of the deep mantle. The possibility of a double crossing of the post-perovskite phase boundary (Hernlund et al., 2005) due to the thermal boundary layer right at the CMB raises an interesting question: if the temperature right at the CMB is hot enough to partially melt perovskite or post-perovskite, should seismic detection of a high and low velocity reflector within D″ (e.g., as in Thomas et al., 2004, which Hernlund et al., 2005, argue for support of the phase boundary double crossing) be accompanied by ULVZ structure? If yes, this has not been detected as of yet, but future work should target better resolution of this possibility. We clarify that the post-perovskite structure in solid phase does not contain any known significant velocity reduction that matches those seen in ULVZ modeling ($\delta V_P \sim -10\%$, $\delta V_S \sim -30\%$).

5 CONCLUSIONS

In this chapter, we have discussed ultra-low velocities at the CMB, and their possible relationship to deep mantle megapiles or superplumes. Certainly, ULVZ structure may have far reaching effects in Earth's global cycles (Muller, 2002; Dobson and Brodholt, 2005). Though important uncertainties still exist in the seismic modeling. For example, in the SPdKS and PKP modeling, the CMB interacts with waves entering and exiting the core. Thus in many cases, large uncertainties exist regarding the exact location of anomalous structures. This can be improved by adding topside CMB reflection probes, like PcP or ScP precursors (e.g., Mori and Helmberger, 1995; Rost et al., 2005), as well as devising new ULVZ probes, like $PKKP^{diff}_{AB}$ (Rost and Garnero, 2006). Another important point is that most ULVZ modeling to date has utilized 1D wave propagation tools (except for a few notable studies, like Wen and Helmberger, 1998a, b). Future studies need to incorporate improvements in this area.

In this chapter we have summarized recent ULVZ findings in relationship to possible dense thermochemical piles in D″, which may be intimately related to superplumes. The large dense piles may explain the degree 2 low shear velocity heterogeneity reveal by seismic tomography, and help to explain several seismic observations, including sharp sides to these structures and marked differences (even anticorrelation) between P and S heterogeneity—neither of which can be explained by thermal anomalies alone. Geodynamical calculations suggest that the hottest deep mantle temperatures are beneath the edges of the dense piles, which is the most likely region to develop ULVZ with origin of partial melt. Topographical ridges to the dense piles near these edges are the most likely geographical regions to form mantle

plumes. While this scenario presents a self-consistent story for ULVZ, large scale low velocities in the deepest mantle, and plume genesis, several important uncertainties are noted, primarily relating to resolution issues in the seismic imaging and geodynamic modeling.

ACKNOWLEDGEMENTS

We are grateful to the Superplume project for the opportunity to participate, M. Hedlin for the PKP scattering map, F. Deschamps and M. Ishii for density perturbation maps, C. Laj for the VGP reversal data, S. Grand, B. Romanowicz, G. Laske, Y. Gu, and J. Ritsema for their δV_S models, C. Lithgow-Bertelloni for the density anomaly locations, and B. Steinberger for the hot spot locations. The authors thank an anonymous reviewer, whose comments helped improve the manuscript. The work was partially funded by NSF Grant EAR-0135119.

REFERENCES

Akins, J.A., S.-N. Luo, P.D. Asimow, and T.J. Ahrens (2004) Shock-induced melting of $MgSiO_3$ perovskite and implications for melts in Earth's lowermost mantle. *Geophys. Res. Lett.*, 31(14), doi:10.1029/2004GL020237.

Bataille, K., and F. Lund (1996) Strong scattering of short-period seismic waves by the core-mantle boundary and the P-diffracted wave. *Geophys. Res. Lett.*, 23, 2413–2416.

Bataille, K., S. Flatté, and R.S. Wu (1990) Inhomogeneities near the core mantle boundary evidenced from scattered waves: A Review. *Pure Applied Geophys.*, 132, 151–173.

Berryman, J.G. (2000) Seismic velocity decrement ratios for regions of partial melt in the lower mantle. *Geophys. Res. Lett.*, 27, 421–424.

Bullen, K.E. (1949) Compressibility-pressure hypothesis and the Earth's interior. *Mon. Not. Roy. Astron. Soc., Geophys. Suppl.*, 5, 355–368.

Bunge, H.P., M.A. Richards, C. Lithgow-Bertelloni, J.R. Baumgardner, S.P. Grand, and B.A. Romanowicz (1998) Timescales and heterogeneous structure in geodynamic Earth models. *Science*, 280, 91–95.

Bunge, H.P., M.A. Richards, and J.R. Baumgardner (2002) Mantle-circulation models with sequential data assimilation: Inferring present-day mantle structure from plate-motion histories. *Phil. Trans. R. Soc. Lond. A*, 360, 2545–2567.

Cormier, V.F. (1999) Anisotropy of heterogeneity scale lengths in the lower mantle from PKIKP precursors. *Geophy. J. Int.*, 136, 373–384.

Cormier, V.F. (2000) D″ as a transition in the heterogeneity spectrum of the lowermost mantle. *J. Geophys. Res.*, 105, 16193–16205.

Davaille, A. (1999) Simultaneous generation of hotspots and superswells by convection in a heterogeneous planetary mantle. *Nature*, 402, 756–760.

Davaille, A., F. Girard, and M. Le Bars (2002) How to anchor hotspots in a convecting mantle? *Earth Planet. Sci. Lett.*, 203, 621–634.

Deschamps F., and J. Trampert (2003) Mantle tomography and its relation to temperature and composition. *Phys. Earth Planet. Int.*, 140, 277–291.

Dobson, D.P., and J.P. Brodholt (2005) Subducted iron formations as a source of ultralow-velocity zones at the core-mantle boundary. *Nature*, 434, 371–374.

Duncan, R.A., and M.A. Richards (1991) Hotspots, mantle plumes, flood basalts, and true polar wander. *Rev. Geophys.*, 29 (1), 31–50.

Dziewonski, A.M. (1984) Mapping the lower mantle: Determination of lateral heterogeneity in *P* velocity up to degree and order 6. *J. Geophys. Res.*, 89, 5929–5952.

Dziewonski, A.M., and D.L. Anderson (1981) Preliminary reference Earth model. *Phys. Earth and Planet. Inter.*, 25(4), 297–356.

Farnetani, C.G., and H. Samuel (2005) Beyond the thermal plume paradigm. *Geophys. Res. Lett.*, 32, No. 7, L07311, 10.1029/2005GL022360.

Flatté, S.M., and R.S. Wu (1988) Small-scale structure in the lithosphere and asthenosphere deduced from arrival-time and amplitude fluctuations at NORSAR. *J. Geophys. Res.*, 93, 6601–6614.

Ford, S.R., E.J. Garnero, and A.K. McNamara (2006) A strong lateral shear velocity gradient and anisotropy heterogeneity in the lowermost mantle beneath the southern Pacific. *J. Geophys. Res.*, 111, B03306, doi:10.1029/2004JB003574.

Garnero, E.J. (2000) Heterogeneity of the lowermost mantle. *Ann. Rev. Earth Planetary Sci.*, 28, 509–537.

Garnero, E.J. (2004) A new paradigm for Earth's core-mantle boundary. *Science*, 304, doi:10.1126/science.1097849.

Garnero, E.J., and D.V. Helmberger (1998) Further structural constraints and uncertainties of a thin laterally varying ultra-low velocity layer at the base of the mantle. *J. Geophys. Res.*, 103, 12495–12509.

Garnero, E.J., V. Maupin, T. Lay, and M.J. Fouch (2004) Variable azimuthal anisotropy in Earth's lowermost mantle. *Science*, 306(5694).

Grand, S.P. (2002) Mantle shear-wave tomography and the fate of subducted slabs. *Phil. Trans. R. Soc. Lond. A*, 360, 2475–2491.

Gu, Y.J., A.M. Dziewonski, W.J. Su, and G. Ekstrom (2001) Models of the mantle shear velocity and discontinuities in the pattern of lateral heterogeneities. *J. Geophys. Research-Solid Earth*, 106(B6), 11169–11199.

Hager, B.H., R.W. Clayton, M.A. Richards, R.P. Comer, A.M. Dziewonski (1985) Lower mantle heterogeneity, dynamic topography and the geoid. *Nature*, 313(6003), 541–546.

Hedlin, M.A.H., and P.M. Shearer (2000) An analysis of large scale variations in small-scale mantle heterogeneity using Global Seismic Network recordings of precursors to PKP. *J. Geophys. Res.*, 105, 13655–13673.

Helmberger, D.V., and S. Ni (2005) Approximate 3D body wave synthetics for tomographic models. *Bull. Seismol. Soc. Am.*, 95, 212–224.

Hernlund, J.W., C. Thomas, and P.J. Tackley (2005) A doubling of the post-perovskite phase boundary and the structure of the lowermost mantle. *Nature*, 434, 882–886.

Ishii, M., and J. Tromp (1999) Normal-mode and free-air gravity constraints on lateral variations in velocity and density of Earth's mantle. *Science*, 285, 1231–1236.

Ishii, M., and J. Tromp (2004) Constraining large-scale mantle heterogeneity using mantle and inner-core sensitive normal modes. *Phys. Earth Plan. Int.*, 146, 113–124.

Jellinek, A.M., and M. Manga (2002) The influence of a chemical boundary layer on the fixity and lifetime of mantle plumes. *Nature*, 418, 760–763.

Jellinek, A.M., and M. Manga (2004) Links between long-lived hotspots, mantle plumes, D″ and plate tectonics. *Rev. Geophys.*, 42(3), RG3002, 10.1029/2003RG000144.

Ji, Y., and H.C. Nataf (1998) Detection of mantle plumes in the lower mantle by diffraction tomography: Theory. *Earth and Planetary Science Letters*, 159(3–4), 87–98.

Kendall, J.-M., and P. G. Silver (1998) Investigating causes of D″ anisotropy. In Gurnis, M., M. Wyession, E. Knittle, and B. Buffet (eds.) The Core-Mantle Boundary Region, AGU, Washington, D.C., USA, pp. 97–118.

Kendall, J.-M., Seismic anisotropy in the boundary layers of the mantle. In Karato, S., A.M. Forte, R.C. Liebermannm, G. Masters, and L. Stixrude (eds.) Earth's Deep Interior: Mineral Physics and Tomography From the Atomic to the Global Scale, AGU, Washington, D.C., USA, pp. 133–159.

Koper, K.D., and M.L. Pyle (2004) Observations of PKiKP/PcP amplitude ratios and implications for Earth structure at the boundaries of the liquid core. *J. Geophys. Res.*, 109, B03301, doi:10.1029/2003JB002750.

Knittle, E., and R. Jeanloz (1989) Simulating the core-mantle boundary: An experimental study of high-pressure reactions between silicates and liquid iron. *Geophys. Res. Lett.*, 16, 609–612.

Knittle, E., and R. Jeanloz (1991) Earth's core-mantle boundary—Results of experiments at high pressures and temperatures. *Science*, 251, 1438–1443.

Kuo, C., and B. Romanowicz (2002) On the resolution of density anomalies in the Earth's mantle using spectral fitting of normal mode data. *Geophys. J. Inter.*, 150, 162–179.

Lay, T., E.J. Garnero, Q. Williams, L. Kellogg, and M.E. Wysession (1998) Seismic wave anisotropy in the D″ region and its implications, In Gurnis, M., M. Wysession, E. Knittle, and B. Buffett (eds.) The Core-Mantle Boundary Region, AGU, Washington, D.C., U.S.A., pp. 299–318.

Lay, T., and E.J. Garnero (2004) Core-mantle boundary structures and processes. In Sparks, R.S.J., and C.J. Hawkesworth (eds.) The State of the Planet: Frontiers and Challenges in Geophysics, Geophysical Monograph 150, IUGG Volume 19, doi:10.1029/150GM04.

Lay, T., E.J. Garnero, and Q. Williams (2004) Partial melting in a thermo-chemical boundary layer at the base of the mantle. *Phys. Earth Planet. Int.*, 146, 441–467.

Lay, T., D. Heinz, M. Ishii, S.-H. Shim, J. Tsuchiya, T. Tsuchiya, R. Wentzcovitch, and D.A. Yuen (2005) Multidisciplinary impact of the deep mantle phase transition in perovskite structure. *Eos Trans.*, 86, No. 1, 1–15.

Lithgow-Bertelloni, C., and M.A. Richards (1998) Dynamics of cenozoic and mesozoic plate motions. *Rev. Geophys.*, 36, 27–78.

Manga, M., and R. Jeanloz (1996) Implications of a metal-bearing chemical boundary layer in D″ for mantle dynamics. *Geophys. Res. Lett.*, 23, 3091–3094.

Maruyama, S. (1994) Plume tectonics. *J. Geol. Soc. Jpn.*, 100, 24–49.

Maruyama, S., M. Kumazawa, and S. Kawakami (1994) Towards a new paradigm on the Earth's dynamics. *J. Geol. Soc. Jpn.*, 100, 1–3.

Masters, G., and D. Gubbins (2003) On the resolution of density within the Earth. *Phys. Earth Planet. Int.*, 140, 159–167.

Masters, G., G. Laske, H. Bolton, and A. Dziewonski (2000) The relative behavior of shear velocity, bulk sound speed, and compressional velocity in the mantle: Implications for chemical and thermal structure. In Karato, S. (ed.) Earth's Deep Interior, AGU Monograph, 117, pp. 63–87.

McNamara, A.K., and S. Zhong (2004a) Thermochemical structures within a spherical mantle: Superplumes or piles? *J. Geophys. Res.*, 109, B07402, doi:10.1029/2003JB002847.

McNamara, A.K, and S. Zhong (2004b) The influence of thermochemical convection on the fixity of mantle plumes. *Earth and Planet. Sci. Lett.*, 222, 485–500.

McNamara, A.K., and S. Zhong (2005) Thermochemical Piles under Africa and the Pacific. *Nature*, 437, 1136–1139.

Mégnin, C., and B. Romanowicz (2000) The three-dimensional shear velocity structure of the mantle from the inversion of body, surface, and higher-mode waveforms. *Geophys. J. Int.*, 143, 709–728.

Montelli, R., G. Nolet, F. Dahlen, G. Masters, E. Engdahl, and S. Hung (2004) Finite-frequency tomography reveals a variety of plumes in the mantle. *Science*, 303, 338–343.

Morgan, W.J. (1971) Convection plumes in the lower mantle. *Nature*, 230, 42–43.

Morgan, W.J. (1972) Deep mantle convection plumes and plate motions. *Am. Assoc. Petrol. Geol. Bull.*, 56(2), 203–213.

Mori, J., and D.V. Helmberger (1995) Localized boundary layer below the mid-Pacific velocity anomaly from a *PcP* precursor. *J. Geophys. Res.*, 100, 20359–20365.

Muller R.A. (2002) Avalanches at the core-mantle boundary. *Geophys. Res. Lett.*, 29(19), 1935, doi:10.1029/2002GL015938.

Murakami, M., K. Hirose, K. Kawamura, N. Sata, and Y. Ohishi (2004) Post-perovskite phase transition in $MgSiO_3$. *Science*, 304, 855–858.

Ni, S., E. Tan, M. Gurnis, and D.V. Helmberger (2002) Sharp sides to the African Superplume. *Science*, 296, 1850–1852.

Ni, S., and D.V. Helmberger (2003a) Ridge-like lower mantle structure beneath South Africa. *J. Geophys. Res.*, 108, No. B2, 2094.

Ni, S., and D.V. Helmberger (2003b) Seismological constraints on the South African superplume; could be the oldest distinct structure on Earth. *Earth Planet. Sci. Lett.*, 206, 119–131.

Niu, F., and L. Wen (2001) Strong seismic scatterers near the core-mantle boundary west of Mexico. *Geophys. Res. Lett.*, 28, 3557–3560.

Oganov, A.R., and S. Ono (2004) Theoretical and experimental evidence for a post-perovskite phase of $MgSiO_3$ in Earth's D″ layer. *Nature*, 430, 445–448.

Olson, P., and C. Kincaid (1991) Experiments on the interaction of thermal convection and compositional layering at the base of the mantle. *J. Geophys. Res.*, 96(B3), 4347–4354.

Poirier, J.-P. (1993) Core-infiltrated mantle and the nature of the D″ layer. *J. Geomag. Geoelectr.*, 45, 1221–1227.

Ritsema, J., and H.J. van Heijst (2000) Seismic imaging of structural heterogeneity in Earth's mantle: Evidence for large-scale mantle flow. *Science Progress*, 83, 243–259.

Rokosky, J.M., T. Lay, E.J. Garnero, and S.A. Russell (2004) High resolution investigation of shear-wave anisotropy in D″ beneath the Cocos Plate. *Geophys. Res. Lett.*, 31, L07605, doi:10.1029/2003GL018902.

Romanowicz, B. (1991) Seismic tomography of the Earth's mantle. *Ann. Rev. Earth Planet. Sci.*, 19, 77–99.

Rondenay, S., and K.M. Fischer (2003) Constraints on localized core-mantle boundary structure from multichannel, broadband SKS coda analysis. *J. Geophys. Res.*, 108(B11), 2537, doi:10.1029/2003JB002518.

Rost, S., and J. Revenaugh (2001) Seismic detection of rigid zones at the top of the core. *Science*, 294, 1911–1914.

Rost, S., and J. Revenaugh (2003) Small-scale ultra-low velocity zone structure resolved by ScP. *J. Geophys. Res. Solid Earth*, 108, 10.1028/2001JB001627.

Rost, S., and E.J. Garnero (2006) Detection of an ultra-low velocity zone at the CMB using diffracted $PKKP_{ab}$ waves. *J. Geophys. Res.*, 111, B07309, doi:10.1029/2005JB003850.

Rost, S., E.J. Garnero, Q. Williams, and M. Manga (2005) Seismic constraints on a possible plume root at the core-mantle boundary. *Nature*, 435, 666–669 (doi:10.1038/nature03620).

Saltzer, R.L., E. Stutzmann, and R.D. Van der Hilst (2004) Poisson's ration beneath Alaska from the surface to the core-mantle boundary. *J. Geophys. Res.*, 109, doi:10.1029/2003JB002712.

Samuel, H., C.G. Farnetani, and D. Andrault (2005) Heterogeneous lowermost mantle: Compositional constraints and seismological observables. In Bass, J., R.D. van der Hilst, J. Matas, and J. Trampert (eds.) Structure Evolution and Composition of the Earth's Mantle, AGU Geophysical Monograph.

Shearer, P.M., M.A.H. Hedlin, and P.S. Earle (1998) PKP and PKKP precursor observations: Implications for the small-scale structure of the deep mantle and core. In Gurnis, M., M.E. Wysession, E. Knittle, B.A. Buffett (eds.) The Core-Mantle Boundary Region, Washington D.C, American Geophysical Union, pp. 37–55.

Shim, S.-H., T.S. Duffy, R. Jeanloz, and G. Shen (2004) Stability and crystal structure of $MgSiO_3$ perovskite to the core-mantle boundary. *Geophys. Res. Lett.*, 31, L10603, doi:10.1029/2004GL019639.

Song, X., and T.J. Ahrens (1994) Pressure-temperature range of reactions between liquid iron in the outer core and mantle silicates. *Geophys. Res. Lett.*, 21, 153–156.

Steinberger, B. (2000) Plumes in a convecting mantle: Models and observations for individual hotspots. *J. Geophys. Res.*, 105, 11127–11152.

Su, W.J., and A.M. Dziewonski (1997) Simultaneous inversion for 3-D variations in shear and bulk velocity in the mantle. *Phys. Earth Planet. Int.*, 100, 135–156.

Tackley, P.J. (1998) Three-dimensional simulations of mantle convection with a thermo-chemical basal boundary layer: D″? In Gurnis, M., M.E. Wysession, E. Knittle, and B.A. Buffett (eds.) The Core-Mantle Boundary Region, American Geophysical Union, Washington, D.C., USA, pp. 231–253.

Tackley, P. (2000) Mantle convection and plate tectonics: Toward an integrated physical and chemical theory. *Science*, 288, 2002–2007.

Tackley, P.J. (2002) Strong heterogeneity caused by deep mantle layering. *Geochem. Geophys. Geosys.*, 3(4), 1024, doi:10.1029/2001GC000167.

Thomas, C., E.J. Garnero, and T. Lay (2004) High-resolution imaging of lowermost mantle structure under the Cocos Plate. *J. Geophys. Res.*, 109, doi:10.1029/2004JB003013.

Thorne, M.S., and E.J. Garnero (2004) Inferences on ultralow-velocity zone structure from a global analysis of SPdKS waves. *J. Geophys. Res.*, 109, B08301, doi:10.1029/2004JB003010.

Thorne, M., E.J. Garnero, and S. Grand (2004) Geographic correlation between hot spots and deep mantle lateral shear-wave velocity gradients. *Phys. Earth Planet. Int.*, 146, 47–63.

To, A., T.B. Romanowicz, Y. Capdeville, and N. Takeuchi (2005) 3D effects of sharp boundaries at the borders of the African and Pacific Superplumes: Observation and modeling. *Earth Planet. Sci. Lett.*, 233, 137–153.

Trampert, J., F. Deschamps, J. Resovsky, and D.A. Yuen (2004) Probabilistic tomography maps chemical heterogenities throughout the mantle. *Science*, 306, 853–856.

Tsuchiya, T., J. Tsuchiya, K. Umemoto, and R.M. Wentzcovitch (2004) Elasticity of post-perovskite $MgSiO_3$. *Geophys. Res. Lett.*, 31, L14603, doi:10.1029/2004GL020278.

van der Hilst, R.D., and H. Kárason (1999) Compositional heterogeneity in the bottom 1000 kilometers of Earth's mantle: Toward a hybrid convection model. *Science*, 283, 1885–1888.

Van Thienen, P., J. van Summeren, R.D. van der Hilst, A.P. van den Berg, and N.J. Vlaar (2005) Numerical study of the origin and stability of chemically distinct reservoirs deep in Earth's mantle. In van der Hilst, R.D., J. Bass, J. Matas, and J. Trampert (eds.) The Structure, Evolution and Composition of Earth's Mantle, AGU, Geophysical Monograph, pp. 117–136.

Vidale, J.E., and M.A.H. Hedlin (1998) Evidence for partial melt at the core-mantle boundary north of Tonga from the strong scattering of seismic waves. *Nature*, 391, 682–685.

Wang, Y., and L. Wen (2004) Mapping the geometry and geographic distribution of a very-low velocity province at the base of the Earth's mantle. *J. Geophys. Res.*, 109, B10305, doi:10.1029/2003JB002674.

Wen, L. (2001) Seismic evidence for a rapidly-varying compositional anomaly at the base of the Earth's mantle beneath the Indian ocean. *Earth Planet. Sci. Lett.*, 194, 83–95.

Wen, L., and D.V. Helmberger (1998a) Ultra-low velocity zones near the core-mantle boundary from broadband PKP precursors. *Science*, 279, 1701–1703.

Wen, L., and D.V. Helmberger (1998b) A 2D P-SV hybrid method and its application to localized structures near the core-mantle boundary. *J. Geophys. Res.*, 103, 17901–17918.

Williams, Q., and E.J. Garnero (1996) Seismic evidence for partial melt at the base of Earth's mantle. *Science*, 273, 1528–1530.

Williams, Q., J.S. Revenaugh, and E.J. Garnero (1998) A correlation between ultra-low basal velocities in the mantle and hot spots. *Science*, 281, 546–549.

Wysession, M.E. (1996) Imaging cold rock at the base of the mantle: The sometimes fate of Slabs? In Bebout, G.E., D. Scholl, S. Kirby, and J.P. Platt (eds.) Subduction: Top to Bottom, American Geophysical Union, Washington, D.C., USA, pp. 369–384.

Wysession, M., T. Lay, J. Revenaugh, Q. Williams, E.J. Garnero, R. Jeanloz, and L. Kellogg (1998) The D'' discontinuity and its implications. In Gurnis, M., M. Wysession, E. Knittle, and B. Buffett (eds.) The Core-Mantle Boundary Region, AGU, Washington, D.C., U.S.A., pp. 273–298.

Wysession, M.E., A. Langenhorst, M.J. Fouch, K.M. Fischer, G.I. Al-Eqabi, P.J. Shore, and T.J. Clarke (1999) Lateral variations in compressional/shear velocities at the base of the mantle. *Science*, 284, 120–125.